Nucleophilic Attack on Phosphate Diesters: A Density Functional Study of In−Line Reactivity in Dianionic, Monoanionic, and Neutral Systems

Xabier Lopez ,*,† Annick Dejaegere,‡ Fabrice Leclerc,§ Darrin M. York,|| and Martin Karplus*,⊥, #

Kimika Fakultatea, Euskal Herriko Unibertsitatea, P.K. 1072, 20080 Donostia, Euskadi, Spain, Laboratoire de Biologie et Génomique Structurales, Ecole Supérieure de Biotechnologie de Strasbourg, 674000 Illkirch, France, Laboratoire de Maturation des ARN et Enzymologie Moléculaire, CNRS-UHP Nancy I UMR 7567, Université Henri Poincaré, Faculté des Sciences, B.P. 239, 54506 Vandoeuvre-lès-Nancy, France, Department of Chemistry, University of Minnesota, 207 Pleasant St. SE, Minneapolis, Minnesota 55455-0431, Department of Chemistry and Chemical Biology, Harvard University, Cambridge, Massachusetts 02138, and Laboratoire de Chimie Biophysique, Institut le Bel, Université Louis Pasteur, 67000 Strasbourg, France

Received: January 19, 2006; In Final Form: April 18, 2006

A density functional study of the hydrolysis reaction of phosphodiesters with a series of attacking nucleophiles in the gas phase and in solution is presented. The nucleophiles HOH, HO^-, CH_3OH, and CH_3O^- were studied in reactions with ethylene phosphate, 2′3′-ribose cyclic phosphate and in their neutral (protonated) and monoanionic forms. Stationary-point geometries for the reactions were determined at the density functional B3LYP/6-31++G(d,p) level followed by energy refinement at the B3LYP/6-311++G(3df,2p) level. Solvation effects were estimated by using a dielectric approximation with the polarizable continuum model (PCM) at the gas-phase optimized geometries. This series of reactions characterizes factors that influence the intrinsic reactivity of the model phosphate compounds, including the effect of nucleophile, protonation state, cyclic structure, and solvent. The present study of the in-line mechanism for phosphodiester hydrolysis, a reaction of considerable biological importance, has implications for enzymatic mechanisms. The analysis generally supports the associative mechanism for phosphate ester hydrolysis. The results highlight the importance for the reaction barrier of charge neutralization resulting from the protonation of the nonbridging phosphoryl oxygens and the role of internal hydrogen transfer in the gas-phase mechanism. It also shows that solvent stabilization has a profound influence on the relative barrier heights for the dianionic, monoanionic, and neutral reactions. The calculations provide a comprehensive data set for the in-line hydrolysis mechanisms that can be used for the development of improved semiempirical quantum models for phosphate hydrolysis reactions.

1. Introduction

Phosphate diesters play a fundamental role in biology, including their role as the backbone of DNA and RNA.[1,2] The chemical properties and reactivity of phosphates determine how these biomolecules are formed and cleaved, and therefore, phosphate diesters have been the subject of numerous theoretical and experimental studies.[3−26] A first approximation to understand phosphate diester reactivity is to characterize the energetics of gas-phase model reactions for which a full quantum mechanical treatment is possible. Of particular interest are studies that cover nucleophilic attack of water or methanol on ethylene phosphate (EP), a model for the transphosphorylation and hydrolysis of RNA chains.

Previous computational studies on nonenzymatic phosphate hydrolysis reactions[3,5,9,11−13,17,23,24,27] have focused mainly on the so-called dianionic and monoanionic reaction mechanisms in which either a negatively charged nucleophile (XO^-; X = H, CH_3) or a neutral one (XOH; X = H, CH_3) attacks an unprotonated phosphate diester molecule (i.e., dimethyl phosphate or ethylene phosphate). Very few of these studies has addressed the effect of the sugar ring on the reaction. The pK_a values of phosphates (typically below 3) suggest that they are ionized in aqueous solution around neutral pH and, hence, are the most likely reactant species in nonenzymatic hydrolysis. However, the protonation state of the phosphate esters in enzymatic hydrolysis, especially of the phosphorane transition states and intermediates, are not clear. Recent experimental and theoretical results suggest that the phosphoranes exhibit significantly elevated pK_a[1] (e.g., a value of 7.9 has been suggested for ethylene phosphorane[27] and 8.6 for $P(OH)_5$[28]). Consequently, it is important also to characterize neutral reaction mechanisms because the charge state of the phosphorus species can play an important role in the enzyme-catalyzed reactions.

In this paper, we extend the scope of previous computational work[16,29] to consider neutral reaction mechanisms and to characterize the effect of the sugar ring at a high level of theory and basis set. We have studied by means of density functional theory the following set of reactions:

$$XO(H) + PO_2(H)(-O-Y-O) \rightarrow XO-PO_2(H) - (O-Y-O(H)) \quad (1)$$

where X can be either hydrogen or methyl, and Y is either C_2H_4

* Corresponding authors. E-mail: xabier.lopez@ehu.es (X.L.); marci@tammy.harvard.edu (M.K.).
† Kimika Fakultatea, Euskal Herriko Unibertsitatea.
‡ Laboratoire de Biologie et Génomique Structurales, Ecole Supérieure de Biotechnologie de Strasbourg.
§ Laboratoire de Maturation des ARN et Enzymologie Moléculaire, Université Henri Poincaré.
|| Department of Chemistry, University of Minnesota.
⊥ Department of Chemistry and Chemical Biology, Harvard University.
Laboratoire de Chimie Biophysique, Institut le Bel, Université Louis Pasteur.

10.1021/jp0603942 CCC: $33.50
Published on Web 05/19/2006

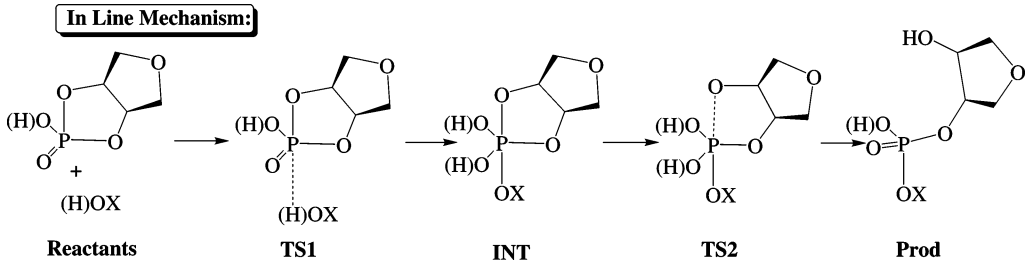

Figure 1. Scheme for the in-line mechanism in phosphate ester hydrolysis.

or a ribose ring. These reactions are illustrated schematically in Figure 1. We restrict the focus to in-line attack mechanisms and do not consider mechanisms that involve pseudorotation. Although exploration and characterization of other mechanisms is important, the formation of the pentacovalent intermediate that results from in-line attack is generally the rate-limiting step.[30,31] Calculations were performed using density functional theory (B3LYP functional) at high basis set levels (6-31++G-(d,p)/6-311++G(3df,2p)). Solvation was approximated by the linear isotropic PCM dielectric continuum model.[32−34]

Nonenzymatic phosphoryl transfer reactions have been studied extensively with quantum chemical methods to quantify the influence of factors that regulate reactivity. Numerous studies have been performed in the gas phase[3−5,17,35] and in solution.[6−10,15,16,18,23,24,26,27,36,37] These studies utilize different levels of electronic structure theory, models for solvation, and other computational protocols that reduce the degree to which meaningful cross-comparisons between studies can be made. The present paper presents calculations for a series of reactions carried out at a consistent level of theory and treatment of solvation that helps unite and extend the results presented previously by different authors with different methods.[4−11,16,23,24,26,27,38−41] Consequently, the results should be of general utility and, in particular, provide a benchmark dataset for the optimization of semiempirical quantum models that can be used in the application of hybrid quantum mechanical/molecular mechanical (QM/MM) methods to study enzymatic phosphate hydrolysis reactions.[29]

2. Methods

2.1. Gas-Phase Calculations. All the structures in the gas phase were optimized with Kohn−Sham density functional theory (DFT) methods, using the hybrid exchange functional of Becke[42] and correlation functional of Lee, Yang, and Parr.[43] Frequency calculations were performed to verify the nature of the stationary points on the potential energy surface (PES); i.e., that there were no imaginary frequencies for minima and only one imaginary frequency for transition states. Geometries and frequencies were determined with a 6-31G++(d,p) basis set. Following geometry optimization, the electronic energies were refined by using a larger 6-311++G(3df,2p) basis set. This basis set is similar to that used in the G2 method,[44,45] which typically yields atomization energies, ionization energies, and relative energies within 1 kcal/mol of the experimental values. All the calculations were done with the GAUSSIAN98 suite of programs.[46]

The B3LYP/6-31G++(d,p) frequencies were used to evaluate the zero-point vibrational energy (ZPVE), thermal vibrational contributions to the enthalpy, entropy, and Gibbs free energy at $T = 298$ K within the harmonic oscillator approximation in the canonical ensemble.[47,48] The rotational and translational energies were treated classically as $^1/_2RT$ per degree of freedom. The thermodynamics relations and energy contributions calculated in the gas phase are:

$$G = H - TS \tag{2}$$

$$H = E + RT \tag{3}$$

$$E = E_0 + E_{\text{vib}} + E_{\text{rot}} + E_{\text{trans}} \tag{4}$$

$$E_0 = E_e + \text{ZPVE} \tag{5}$$

where G, E, H, S, and T are the Gibbs free energy, the energy, the enthalpy, the entropy, and the temperature ($T = 298$ K), respectively, and E_e, E_{vib}, E_{rot}, and E_{trans} are the electronic, thermal vibrational, rotational, and translational energy components, respectively. All quantities except E_e and ZPVE have an explicit temperature dependence.

It is known that anionic and specially dianionic systems are sensitive to basis set choice. For the dianionic phosphoranes considered here, minimal basis sets lead to artificial stabilization of phosphorane intermediates due to basis set superposition errors.[9] Including diffuse functions in the basis set, such as is done here, avoids this artificial stabilization.[9] Although the energetics of the gas phase reactions could be somewhat modified by using different sets of diffuse and polarization functions, the effects should be small compared to the overall reaction energetics and would not affect the conclusion of calculations; see, for example, a study of electron affinity of monoanions where basis sets were extensively compared for monoanionic and dianionic species.[49]

Concerning the evaluation of thermodynamics functions, recent ab initio calculations have indicated that the rigid rotor−harmonic oscillator approximation[50] may lead to an overestimation of the entropic contribution to the activation free energies in phosphate hydrolysis[51,52] Although using a hindered rotor approximation or empirical corrections[52] will affect the absolute values of the activation barriers for the different reactions, it is not expected to affect significantly the relative values for the different charged species (dianionic, monoanionic, and neutral), which is our main purpose.

2.2. Solvation Calculations. Solvent effects were treated by using the polarizable continuum model (PCM).[32−34] In this model, the solute molecule is embedded in a cavity of unit dielectric that is surrounded by solvent modeled by a dielectric continuum. The cavity was defined by using the UAHF sets of radii.[53] The solute and solvent are coupled by a reaction potential of the dielectric medium in response to the solute charge distribution. The polarization of the solvent is represented by a charge density σ introduced on the surface $\mathcal{S}$ of the cavity surrounding the solute, and the corresponding reaction field potential takes the form

$$\phi(\mathbf{r}) = \int_S \mathrm{d}^2 s \frac{\sigma(\mathbf{s})}{|\mathbf{r} - \mathbf{s}|} \tag{6}$$

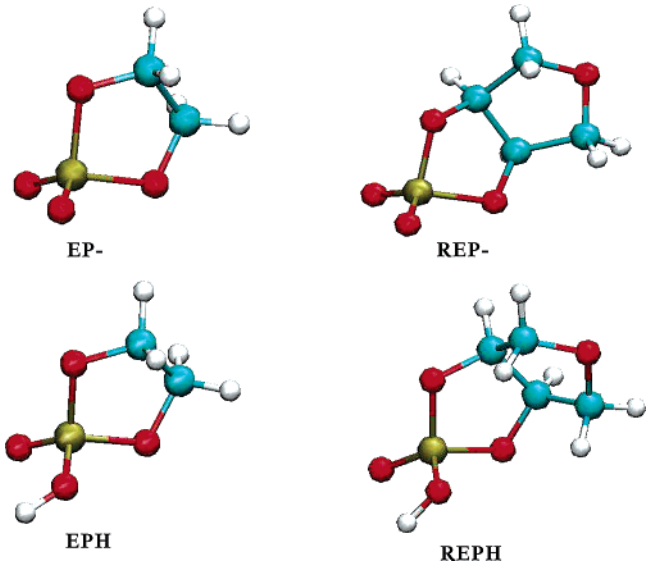

Figure 2. Phosphate reactants: Ethylene phosphate (EP^-), protonated ethylene phosphate (EPH), 2′,3′-ribose cyclic phosphate (REP), and protonated 2′,3′-ribose cyclic phosphate (REPH).

To check the sensitivity of solvation corrections to the method and basis set choice, the solvation calculations were performed with two different electronic structure methods (HF and B3LYP) and two different basis sets (6-31G(d) and 6-31+G(d)), for a total of four combinations of theory/basis set (HF/6-31G(d), HF/6-31+G(d), B3LYP/6-31G(d), and B3LYP/6-31+G(d)). The free energy in solution was calculated as a solvation free energy correction to the gas-phase free energy as:

$$G_{aq} = G_{gas} + \Delta G_{sol} \quad (7)$$

where ΔG_{sol} is the solvation free energy calculated as the difference between the electronic energies in solution and the gas phase plus the self-energy of the solvent reaction field along with an empirical term that account for the nonelectrostatic contributions to the solvation free energy (sometimes referred to as the "cavitation" term).[32,54] The solution free energies of the gas-phase stationary points from eq 7 are then used to estimate the relative energies of the various stationary points in solution, ΔG^i_{aq}, with respect to the energies in solution of the separate reactants. The relative values in solution with respect to the reactant are less affected by the basis set and method choice than absolute solvation energy values, so that the shape of the potential energy surface in solution is similar for the different methods tested. Therefore, and for the sake of brevity, we chose only one method, HF/6-31+G*, to report aqueous free energies; the results obtained with the other methods are given as Supporting Information.

Because of the large number of structures considered, the solvation free energies were calculated at the gas-phase B3LYP/6-31G++(d,p) geometries rather than performing geometry optimizations in solution. Nonetheless, the gas-phase geometry/continuum dielectric approximation employed here provides important insights into how solvent affects the reaction energetics.[9−11] The present calculations do neglect explicit solvent water molecules, which could catalyze the intramolecular proton transfer from phosphoryl oxygens to departing nucleophiles/leaving groups in monoanionic and neutral reactions. Water-mediated proton transfer has been claimed to facilitate formation/cleavage of phosphoranes.[55]

2.3. Nomenclature. To label the different structures along the reaction profile, we introduce the following notation. There are reactants (REAC), hydrogen-bonded complexes (HB), products (PROD), and pentacovalent phosphorane intermediates (INT) that are identified as minima on the potential energy surface, as well as several transition states (TS1, TS2, and TSINT). The name TS1 refers to the transition state for the approach of the nucleophile to the phosphate reactant, while TS2 refers to the transition state for the endocyclic cleavage, which connects the phosphorane intermediates to the products. TSINT refers to transition states that connect different phosphorane intermediates (see Results and Discussion section for details).

The number of stationary points identified on the potential energy surface differs for the dianionic, monoanionic and neutral reactions. In the case of dianionic reactions, there are only REAC, TS1, and PROD structures. In the case of monoanionic and neutral reactions, there are more possibilities, and the nomenclature is detailed below.

2.3.1. Monoanionic Reactions. In the case of water attack on ethylene phosphate, we have considered two type of intermediates (Int_a and Int_b), which differ in the orientation of the equatorial proton (see Figure 4). Considering that the five-membered ring in ethylene phosphate is not planar, the two

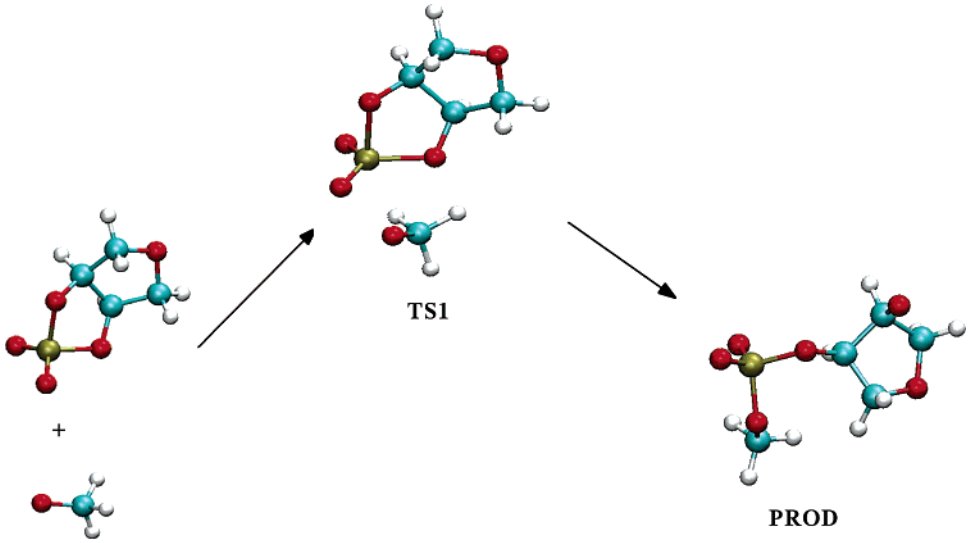

Figure 3. Dianionic potential energy surface. B3LYP/6-31++G(d,p) optimized geometries of the separate reactants, transition state, and product for the in-line methoxide attack on ribose ethylene phosphate.

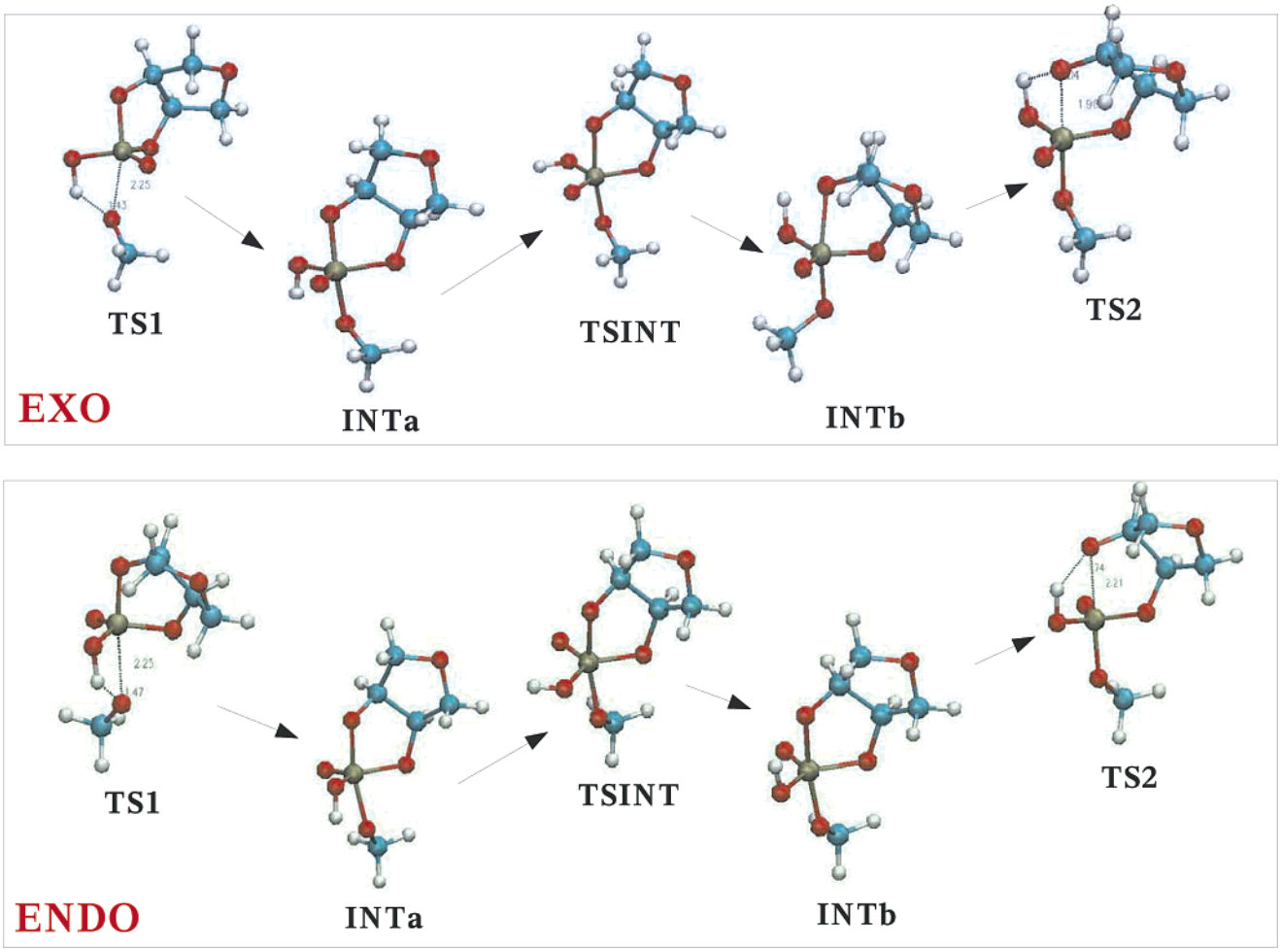

Figure 4. Monoanionic potential energy surface. B3LYP/6-31++G(d,p) optimized geometries of transition states and intermediates for the in-line methanol attack on ribose ethylene phosphate.

equatorial phosphoryl oxygen are not equivalent, so that there are two Int_a and two Int_b structures. However, preliminary calculations showed almost equivalent energetics (within 1 kcal/mol) and similar structures when protonating one or the other oxygen, so that only one structure will be discussed here.

For the reaction with ribose ethylene phosphate, there are more isomers according to whether the protonated phosphoryl oxygen is exo or endo with respect to the ribose ring. These two possibilities were specifically considered, and we distinguish both structures with an exo and endo superscript (see Figure 4).

2.3.2 Neutral Reactions. In the neutral reactions, the stationary points identified are also reactants (REAC), hydrogen-bonded complexes (HB), transition states (TS), phosphorane intermediates (INT), and products (PROD). However, the number of different isomers is larger, as the equatorial oxygens are both protonated and each proton can assume different orientations. In this case, we have introduced two subscripts that take into account the orientation of each of the equatorial protons. The symbol d refers to "down" orientation of the equatorial proton according to the structures of Figure 5, meaning that this proton is oriented toward the oxygen of the nucleophile. The subscript u refers to the "up" orientation, i.e., proton oriented toward the axial endocyclic oxygen (i.e., the oxygen of the leaving group). As shown in Figure 5, we use two subscripts in each case, the first one refers to the orientation of the proton bound to the exo phosphoryl oxygen, and the second one corresponds to the equatorial proton bound to the endo oxygen (exo or endo with respect to the ribose ring).

3. Results and Discussion

The results of DFT calculations for the series of phosphate hydrolysis reactions are presented and discussed. The section is organized into three main subsections that focus on dianionic, monoanionic and neutral reactions, respectively. Each of these subsections examines structures, and thermodynamic quantities in the gas phase and in solution. Particular attention is paid to the geometries of the phosphorane intermediates and the transition states corresponding to the formation of the exocyclic P−O apical bond, the overall rate-limiting transition state in all cases, and to the specific protonation states that give rise to possible phosphorane isomers.

3.1. Dianionic Reaction Mechanism. *3.1.1. Gas-Phase Profile.* The dianionic reaction mechanism corresponds to the attack of the anionic reactant (hydroxide or methoxide) on the negatively charged phosphodiesters, ethylene phosphate and 2,′3′-ribose ethylene phosphate. These are the small molecule models for mechanisms frequently proposed for enzymatic phosphate hydrolysis, where the attack of an activated nucleophile (for example, deprotonated hydroxyl) occurs on the phosphate diester in its physiological anionic protonation state. This reaction has been studied previously on simpler model systems lacking the ribose ring,[3,9−11,16,18] and the global features of the reaction profiles presented here (cf. Figure 3 and Table 1) are in accord with previous studies in that hydrolysis proceeds via direct in-line nucleophilic displacement with inversion of configuration at the phosphorus. The rate-limiting transition state occurs early in the reaction, with distances between the

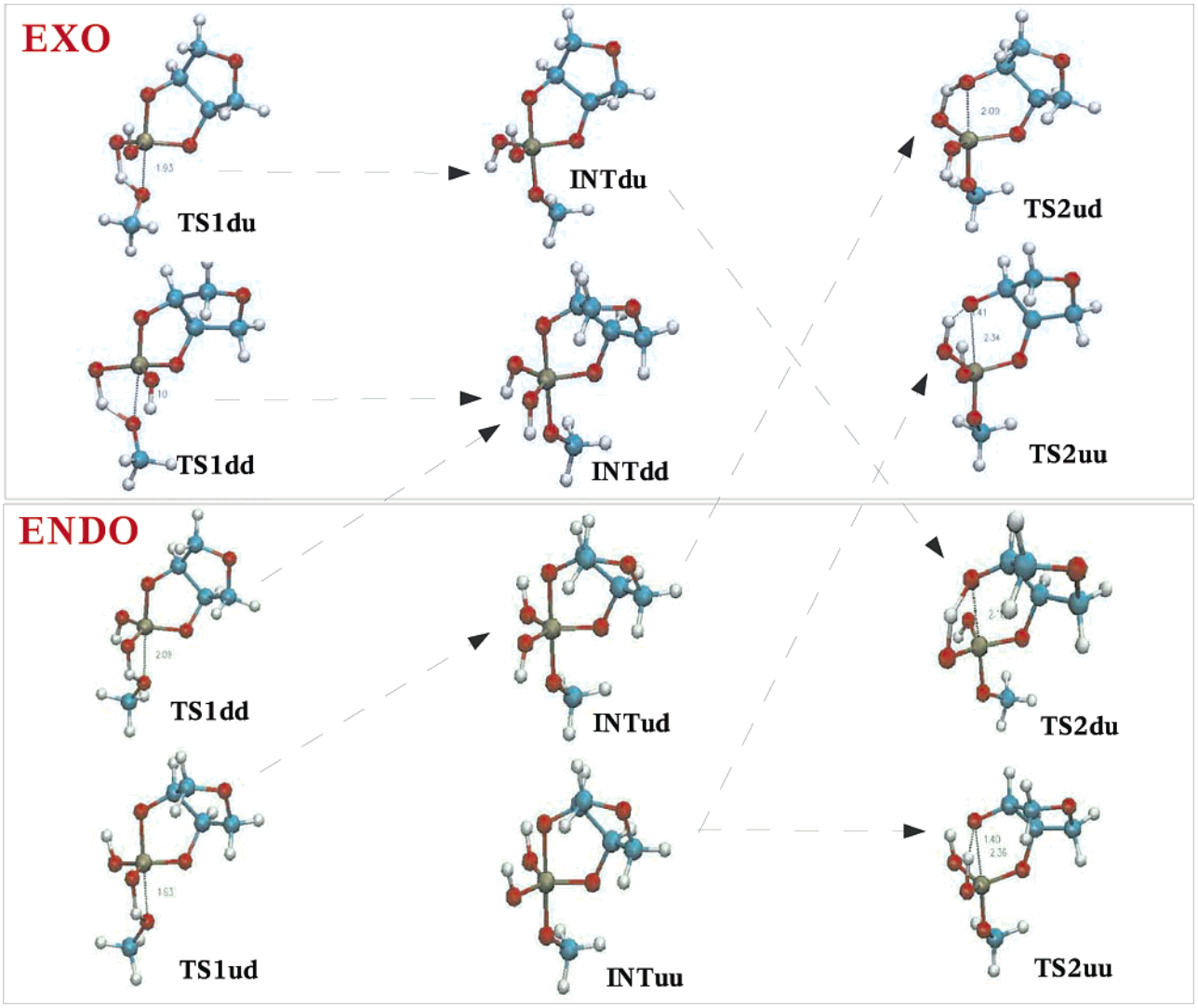

Figure 5. Neutral potential energy surface. B3LYP/6-31++G(d,p) optimized geometries of transition states, and intermediates that correspond to the in-line mechanism of the nucleophilic attack of methanol on 2p,3p-cyclic ribose ethylene phosphate. The dd, du, ud, and uu superscripts refers to the orientation (up or down) of the equatorial protons.

TABLE 1: Dianionic Reactions: Relative Energies in the Gas-Phase with Respect to the Separate Reactants for the XO^- + EP^-/REP^- Reactions (X = CH_3, H; REP = 2′,3′-Cyclic Ribose Ethylene Phosphate, EP^- = Ethylene Phosphate)[a]

	reaction: HO^- + EP^-					reaction: HO^- + REP^-				
	ΔE_e	ΔE_0	ΔH	ΔG	ΔG_{aq}	ΔE_e	ΔE_0	ΔH	ΔG	ΔG_{aq}
TS1	86.71	87.14	86.43	95.94	43.46	81.32	81.80	81.14	90.56	54.11
PROD	35.88	37.00	36.60	44.89	20.45	38.89	39.77	39.34	47.85	23.10

	reaction: CH_3O^- + EP^-					reaction: CH_3O^- + REP^-				
	ΔE_e	ΔE_0	ΔH	ΔG	ΔG_{aq}	ΔE_e	ΔE_0	ΔH	ΔG	ΔG_{aq}
TS1	87.17	87.31	87.13	98.33	44.07	81.97	82.12	82.05	92.98	45.83
PROD	44.10	46.34	46.51	56.64	19.83	49.16	51.14	51.33	61.63	25.18

[a] Numbers are in kcal/mol. E_e corresponds to the electronic energy calculated at our best level of theory (see Methods). Contributions from zero-point vibrational energy, enthalpy, and entropy are estimated at B3LYP/6-31++G(d,p). Last column for each reaction type corresponds to the relative free energy in aqueous solution ΔG_{aq}, obtained from the sum of ΔG_{gas} and the $\Delta\Delta G_{sol}$ solvent contributions (see Methods) evaluated at HF/6-31+G*.

TABLE 2: P−O Axial Bond Distances (Å) and Angle (deg) for All the Stationary Points Characterized for the XO^- + (R)EP^- Reactions Using B3LYP/6-31+G(d,p) Level of Theory

	HO^- + EP^-			HO^- + REP^-		
	P−OX	P−OC	O_{ax}−P−O_{ax}	P−OX	P−OC	O_{ax}−P−O_{ax}
TS1	2.627	1.834	163.07	2.645	1.846	162.9
PROD	1.700	5.136	91.4	1.700	4.264	103.9
	CH_3O^- + EP^-			CH_3O^- + REP^-		
	P−OX	P−OC	O_{ax}−P−O_{ax}	P−OX	P−OC	O_{ax}−P−O_{ax}
TS1	2.627	1.834	163.07	2.645	1.846	162.9
PROD	1.700	5.136	89.6	1.707	4.599	108.6

phosphorus and the incoming nucleophile oxygen around 2.645 Å (cf. Table 2) and an endocyclic P−O_{ax} distance of 1.846 Å. The reaction proceeds directly from the transition state to the products without formation of stable pentacovalent dianionic phosphorane intermediates. In the P−O_{ax} distance range where stable intermediates are observed for the monoanionic and neutral reactions (see below), the potential energy surface is rather flat, but no stationary point was identified. Thus, even if shallow intermediates exist, they are not kinetically significant.[56] This type of mechanism is consistent with kinetic ^{18}O isotope effects[55] for the cleavage reaction of uridine 3′-*m*-nitrobenzyl phosphate (i.e., the reverse transesterification reaction to the methanolysis of cyclic phosphate diesters discussed in the present work), supportive of a concerted-type mechanism but with a late transition state (that is, equivalent to our early-type

transition state for the methanolysis reaction of the cyclic phosphodiester). In addition, on the basis of leaving group effects, highly negative values for β_{lg} (slope of Bronsted-type plots) in the case of the hydroxide ion catalyzed transesterification cleavage of uridine 3′-alkyl phosphates[57−59] have been reported, suggesting that, at the transition state, the departure of the corresponding alkoxide group is almost complete, which is again in agreement with an early transition state for the methanolysis of cyclic phosphodiesters. It must be noted that a break in the Bronsted-type free energy relationship has been recently reported[59] for the alkaline cyclization of uridine 3′-phosphate esters at pK_a values of the leaving group (the nucleophile in our case) lower than the pK_a of the 2′ oxyanion nucleophile. This can be linked to a change in the rate-determining transition state as the basicity of the leaving group (the nucleophile in our case) increases, which is coherent with our data.

The dianionic reaction has a very high activation energy barrier in the gas phase; it is of the order of 87 (ethylene phosphate) to 81 (2′,3′-ribose ethylene phosphate) kcal/mol (see Table 1). The free energy barrier is higher by 9−10 kcal/mol, which reflects the loss of translational and rotational degrees of freedom in the dianionic complexes, and the inclusion of vibrational entropic contributions does not significantly affect the shape of the reaction path. The high activation barrier results largely from the Coulombic repulsion between the two negatively charged ions in the gas phase.[9−11] The presence of the ribose ring lowers the activation barrier by 5 kcal/mol with respect to ethylene phosphate, presumably due to its better ability to delocalize the electronic charge and reduce the Coulomb repulsion of the dianion. Overall, the hydrolysis reaction is endothermic in the gas phase. The nature of the attacking group (methoxide vs hydroxide) influences the reaction energetics for the hydrolysis; i.e., when methoxide is the nucleophile, the reaction is more endothermic by over 10 kcal/mol (see Table 1). This can be linked to the greater stability of the methoxide reactant relative to hydroxide. The effect of the ribose ring is fairly small with respect to the barrier height and overall reaction energetics. It can be noted that the backward reaction, i.e., that from the products to reactants, and methoxide is a model for the transphosphorylation step of RNA hydrolysis. From the data presented here, the activation energy for this particular reaction is 32.8 kcal/mol, which is significantly less than that for the hydrolysis. The activation energy for the backward hydrolysis reaction is higher (42.4 kcal/mol) when hydroxide is the leaving group, as expected, because hydroxide is a worse leaving group than methoxide in bearing a negative charge in the gas phase.

3.1.2. Solution Profile. To obtain a first approximation to the reaction profile in solution, we estimated the solvation free energies (G_{sol}) of the gas-phase stationary points with the continuum dielectric (PCM-UAHF) methods, as discussed in Section 2.2 (Tables 1, S9, S10, and S11).

It can be seen that, for the dianionic reaction, the solvation free energy of the separate reactants is significantly less favorable than that of the transition state and product. This is in accord with the expectation that a dianionic species is more favorably solvated than two monoanionic reactants.[11] The large favorable solvation of dianionic transition states leads to a significant reduction of the activation barrier in solution. The barrier is lowered to 45−55 kcal/mol depending on the nature of the reactants. In the gas phase, the activation barrier for the reaction was somewhat lower, while as the transition states for the compounds are bulkier, they are less well solvated, and therefore, the estimated barriers in solution for the reactions are similar or even somewhat higher than those obtained for ethylene phosphate. A detailed comparison of the solution barriers for the various reactants and nucleophiles would necessitate obtaining stationary points in solution. Nevertheless, the current data indicate that the barriers are similar for all reactions.

These data also highlights the importance of the consideration of the solvent to understand the hydrolysis reactions, as noted in earlier studies.[10,11] For the reverse (i.e., transphosphorylation) reaction, the effect of solvation on the activation barrier is quantitatively much less important than for the hydrolysis step, as the reactants are also dianionic; solvation reduces the activation barrier by about 10 kcal/mol. The difference in solvation free energies with the different methods employed tend to cancel out when calculating relative energies. This can be seen in Figure 7, where we depict the values of the solvation free energies for the different species calculated at HF/6-31+G*, B3LYP/6-31G*, and B3LYP/6-31+G* versus the HF/6-31G* values. The inclusion of diffuse functions tend to slightly increase the solvation free energy (in absolute value), whereas the B3LYP method has a larger effect and gives smaller (in absolute value) solvation free energies than Hartree−Fock in all cases. However, these trends are consistent for all the structures treated, and hence, the barriers calculated in solution with the different methods are similar. As stated in the Methods section, only HF/6-31+G* numbers are included in Tables 1, 3, and 6.

3.2. Monoanionic Reaction Mechanism. *3.2.1. Gas-Phase Profile.* Monoanionic reactions correspond to either the attack of an activated nucleophile (i.e., OH^- or CH_3O^-) on the neutral phosphate or to the attack of a neutral nucleophile (water or methanol) on the phosphate in its usual charge state (−1). Monoanionic reactions have been proposed in enzymatic systems[60] where the attack of an incoming charged nucleophile would be accompanied by a proton transfer from a nearby general acid to the phosphate, which would facilitate the attack.

For the reactions considered here, in the gas phase, identical stationary points are obtained for the attack of an anionic nucleophile on the neutral phosphate and the attack of the neutral nucleophile on the anionic phosphate, so that, except in the reactant stage, the potential energy surfaces are identical. The initial step in the gas-phase reaction for the attack of water (or methanol) on the monoanionic phosphates is the formation of an H-bonded complex between the reactants (see Table 3 and Figure 4). The stability of the hydrogen-bonded complex is quite significant in the gas phase due to favorable electrostatic interactions (−15.5 kcal/mol in energy), but the entropic contribution to complex formation is unfavorable, as expected, and hence, in free energy, the stability is only −3.3 kcal/mol (Table 3). The geometry of the complex differs if water or methanol is used as the nucleophile; with water, two slightly elongated hydrogen bonds are formed with the nonbridging phosphoryl oxygens (approximately 2.1 Å), whereas CH_3OH forms a single strong hydrogen bond (approximately 1.75 Å). If the reactants used for initial gas-phase geometry optimization are the neutral phosphate and anionic nucleophile, no stable complex is formed where the phosphate oxygen is the H-bond donor. This is expected from the relative gas-phase proton affinities of the reactants; i.e., when the neutral phosphate and anionic nucleophile interact, a proton transfer occurs and the only stable H-bonded complex that can be identified correspond to the neutral nucleophile donating the H-bond to the anionic phosphate oxygen.

As the reaction proceeds to the rate-limiting transition state, the proton forming the hydrogen bond is transferred from the

TABLE 3: Monoanionic Reaction: Relative Energies in the Gas-Phase with Respect to the Separate Reactants for the XOH + EP$^-$/REP$^-$ Reactions (X = CH_3, H)[a]

	reaction: HOH + EP$^-$					reaction: CH_3OH + EP$^-$				
	ΔE_e	ΔE_0	ΔH	ΔG	ΔG_{aq}	ΔE_e	ΔE_0	ΔH	ΔG	ΔG_{aq}
HB	−15.27	−12.82	−13.36	−4.59	8.93	−14.65	−13.49	−13.22	−4.86	7.50
TS1	22.88	23.73	22.23	34.26	42.14	21.84	21.29	20.63	32.96	41.94
Int_a	13.34	16.45	15.07	27.12	26.68	13.73	15.44	14.77	27.85	30.72
TSINT						22.65	23.26	22.52	35.58	35.77
Int_b	13.76	16.29	15.24	26.32	25.88	13.73	15.44	14.77	27.85	30.72
TS2	13.70	15.83	14.35	26.37	29.50	13.78	14.78	13.85	27.29	31.90
PROD	−19.36	−16.33	−17.31	−6.76	0.88	−19.35	−17.52	−17.84	−6.32	6.72
XO^- + EPH	61.02	60.98	60.96	62.06	13.71	52.11	49.71	49.72	50.24	15.61
	reaction: HOH + REP$^-$					reaction: CH_3OH + REP$^-$				
	ΔE_e	ΔE_0	ΔH	ΔG	ΔG_{aq}	ΔE_e	ΔE_0	ΔH	ΔG	ΔG_{aq}
HB	−14.51	−11.94	−12.53	−3.29	10.27	−14.00	−12.68	−12.47	−3.62	9.18
$TS1^{Exo}$	24.48	25.07	23.66	35.33	39.53	23.64	22.80	22.24	34.18	43.96
$TS1^{Endo}$	24.28	25.08	23.64	35.40	39.56	23.42	22.86	22.25	34.45	43.18
Int_a^{Exo}	13.64	16.57	15.31	26.98	26.48	14.70	16.05	15.57	27.96	29.27
Int_a^{Endo}	13.65	16.51	15.33	26.71	27.34	13.49	15.04	14.51	27.10	29.78
$TSINT^{Exo}$						23.24	23.60	23.01	35.69	34.78
$TSINT^{Endo}$	14.51	16.92	15.49	27.34	26.75	22.41	22.90	22.28	34.90	35.58
Int_b^{Exo}	13.02	15.86	14.74	26.01	28.33	13.98	15.54	15.03	27.61	31.45
Int_b^{Endo}	13.65	16.51	15.33	26.71	27.34	13.49	15.04	14.51	27.10	29.78
$TS2^{Exo}$	13.99	15.93	14.56	26.19	30.51	14.23	14.96	14.23	26.86	30.96
$TS2^{Endo}$	13.69	15.65	14.27	25.97	28.45	13.79	14.58	13.81	26.75	31.73
PROD	−14.49	−11.93	−12.75	−2.77	8.27	−14.43	−12.96	−13.15	−2.04	9.55
XO^- + REPH	65.79	65.45	65.00	66.98	14.15	56.88	54.18	53.76	55.17	16.06

[a] Numbers are in kcal/mol. E_e corresponds to the electronic energy calculated at our best level of theory (see Methods). Contributions from zero-point vibrational energy, enthalpy, and entropy are estimated at B3LYP/6-31++G(d,p). Last column for each reaction type corresponds to the relative free energy in aqueous solution (ΔG_{aq}), obtained from the sum of ΔG_{gas} and the $\Delta\Delta G_{sol}$ solvent contributions (see Methods) evaluated at HF/6-31+G*.

nucleophile to one of the nonbridging phosphoryl oxygens. This proton transfer is almost complete in the transition state, as the distance between the incoming O and the proton (1.4−1.5 Å) is significantly longer than the distance between the phosphoryl O_{phos} and the hydrogen (1.0−1.1 Å). The H−O−H angle, however, deviates significantly from linearity (134−137°, see Table 5), and the O− −O distance (proton donor and acceptor) is between 2.308 and 2.325 Å. Experimental results on cleavage and isomerization of RNA phosphodiester bonds[58,61,62] suggests a similar mechanism in which the rate-limiting transition state corresponds to exocyclic cleavage of the phosphorane concerted with proton transfer to the departing alkoxide. In this sense, it has been shown that, in the case of phosphorane monoanionic triesters, for which intramolecular proton transfer from the phosphoryl oxygen to the leaving group is not an option, isomerization is 10^5 times faster than the cleavage. However, in phosphorane diesters, isomerization is only 1−2 orders of magnitude faster than cleavage. Besides, also consistent with a proton transfer to the leaving group concerted with the rate-limiting bond rupture, the experimental[61] β_{lg} of the cleavage is only moderately negative, −0.59, as compared with the high negative value for the hydroxide-ion-catalyzed reaction of phosphodiester monoanions,[57] −1.28, in which the alkoxide departs unprotonated.

In general, there are large departures from the ideal 180° in the O_{ax}−P−O_{ax} angle in the transition state; values between 159° and 164° are obtained (Table 4). Regarding the distance between the nucleophile and the phosphorus in TS1, they are all very similar, 2.235−2.265 Å, with slightly longer P−OX distances for methanol than for water. For the attack on 2′,3′-ribose ethylene phosphate, the P−OX distances in the transition state are shorter than that for ethylene phosphate. The transition states TS1s of the monoanionic reactions are more associative than the transition states of the dianionic reactions in which the values of P−OX and P−OC distances at TS1 were longer than in the present case. Because of the geometry of the phosphate reactant, the two nonbridging equatorial oxygens are not equivalent, so that two transition states are identified (labeled exo and endo for 2′,3′-ribose ethylene phosphate as a reactant,

TABLE 4: P−O Axial Bond Distances (Å) and Angle (deg) for All the Stationary Points Characterized for the XOH + (R)EP$^-$ Reactions Using B3LYP/6-31+G(d,p) Level of Theory

	HOH + EP$^-$			CH_3OH + EP$^-$		
	P−OX	P−OC	O_{ax}−P−O_{ax}	P−OX	P−OC	O_{ax}−P−O_{ax}
HB	3.391	1.694	134.0	3.845	1.696	127.7
TS1	2.254	1.713	163.6	2.265	1.713	161.7
Int_a	1.787	1.779	168.4	1.790	1.780	160.4
TSINT				1.743	1.819	161.2
Int_b	1.703	2.005	164.1	1.715	1.893	160.9
TS2	1.688	2.153	162.8	1.689	2.149	160.4
PROD	1.612	3.414	150.8	3.528	1.671	104.5
	HOH + REP$^-$			CH_3OH + REP$^-$		
	P−OX	P−OC	O_{ax}−P−O_{ax}	P−OX	P−OC	O_{ax}−P−O_{ax}
HB	3.390	1.690	130.8	3.854	1.690	121.8
$TS1^{Exo}$	2.237	1.718	161.2	2.254	1.717	159.0
$TS1^{Endo}$	2.240	1.716	163.7	2.248	1.715	162.0
Int_a^{Exo}	1.784	1.777	168.8	1.788	1.787	165.2
Int_a^{Endo}	1.772	1.788	163.1	1.777	1.787	159.3
$TSINT^{Exo}$				1.747	1.835	168.7
$TSINT^{Endo}$	1.735	1.824	159.2	1.733	1.824	159.3
Int_b^{Exo}	1.703	1.921	163.0	1.711	1.911	160.2
Int_b^{Endo}	1.704	1.911	162.9	1.706	1.909	159.3
$TS2^{Exo}$	1.675	2.240	162.5	1.673	2.254	159.9
$TS2^{Endo}$	1.678	2.218	161.9	1.678	2.213	159.8
PROD	1.653	3.421	117.1	1.648	3.411	121.6

TABLE 5: Proton Transfer between Oxygens at the Transition States

	HOH + EP^-					CH_3OH + EP^-				
	$H-O_X$	$H-O_P$	$H-O-CH_2^-$	O−O	∠O−H−O	$H-O_X$	$H-O_P$	$H-O-CH_2^-$	O−O	∠O−H− O
TS1	1.430	1.072		2.325	136.7	1.467	1.050		2.322	134.5
TS2		0.986	1.746	2.335	120.4		0.985	1.748	2.336	120.3
	HOH+REP^-					CH_3OH + REP^-				
	$H-O_X$	$H-O_P$	$H-O-CH_2^-$	O−O	∠O−H−O	$H-O_X$	$H-O_P$	$H-O-CH_2^-$	O−O	∠O−H− O
$TS1^{Exo}$	1.401	1.085		2.314	136.8	1.429	1.065		2.308	135.1
$TS1^{Endo}$	1.428	1.073		2.325	136.2	1.465	1.052		2.323	134.1
$TS2^{Exo}$		0.992	1.699	2.408	124.9		0.992	1.695	2.410	125.1
$TS2^{Endo}$		0.986	1.730	2.408	122.5		0.985	1.737	2.411	122.2

see Figure 4). However, there is very little difference in the activation barriers and overall geometries between the two structures.

The gas-phase energy barrier between the reactants (taken as the neutral nucleophile and charged phosphate) and rate-limiting transition state are 21−25 kcal/mol, while the corresponding free energy barriers are 32−35 kcal/mol (see Table 3). The barriers with respect to the stable hydrogen-bonded complex are, of course, higher, but in free energy, the difference is only about 3 kcal/mol. For instance, in the case of a methanol attack on 2′,3′-ribose ethylene phosphate, the gas-phase free energy barrier with respect to separated methanol and charged phosphate is 34.2 kcal/mol for $TS1^{Exo}$, while the barrier with respect to the hydrogen-bonded complex is 37.8 kcal/mol. It is also possible to consider taking the anionic nucleophile and neutral phosphate as the reference energy. However, these reactants are much higher in energy than the charged phosphate and neutral nucleophile (by 50−65 kcal/mol in the gas phase, see Table 3). In solution, the difference in energy is less (see Table 3, the anionic nucleophile and neutral phosphate are only about 10−15 kcal/mol higher than the negative phosphate and neutral nucleophile)), but the lowest energy species remains the neutral nucleophile and anionic phosphate, as expected. It is thus clear that, in the gas phase, the activation barrier is significantly lower for the monoanionic reaction than for the dianionic one.

The potential energy surface for the monoanionic reaction is more complex than for the dianionic one. Indeed, as the reaction proceeds from the exocyclic transition state, stable pentacovalent compounds are formed (i.e., phosphoranes). They are the intermediates of the reaction, and they have a distorted trigonal bipyramid structure. The central phosphorus atom is bound to five oxygens, two of them occupying axial positions (O_{ax}) and other three occupying equatorial positions. These intermediates are higher in energy than the reactants by 13−15 kcal/mol (see Table 3). For the monoanionic reaction of 2′,3′-ribose ethylene phosphate, four of these intermediates can be identified (cf. Figure 4) that differ in the position and relative orientation of the proton bound to the equatorial oxygens. Indeed, the proton can be bound to each equatorial oxygen, as these are not equivalent (labeled exo and endo, cf. Figure 4). The proton can then be oriented either toward the incoming nucleophile oxygen (Int_a) or toward the departing leaving group oxygen (Int_b, Figure 4).

These stable intermediates occur at different stages on the reaction pathway. In the transition state of nucleophilic attack (TS1), the proton that has been transferred from the incoming nucleophile is still oriented toward it, and this orientation is kept in the subsequent intermediate (Int_a). A rotation of the equatorial proton then occurs, leading to the transition state (TSINT, cf. Figure 4) where the proton is situated in the equatorial plane. This transition state is associated with a significant barrier of about 10 kcal/mol with respect to the intermediates and show similar gas-phase energies to those of the transition states for nucleophilic attack (see Table 3). This rotation of the proton bound to the equatorial oxygen is an interesting feature of the gas-phase potential energy surface. The barrier for rotation of the proton is wide enough that the probability of tunneling is negligible.

In the case of water as the nucleophile, the rotation of the proton is coupled to pseudorotation of the phosphorane intermediate. This type of coupling between the rotation of the P−OH bonds and pseudorotation has also been identified in the past.[63] Therefore, a transition state for pure proton rotation cannot be identified as a stationary point on the potential energy surface. A discussion of pseudorotation mechanisms[25] is beyond the scope of the present paper, and we did not characterize this transition state further. A similar feature had been noticed by Tole and Lim[5,6] in their early studies of hydroxyl ion attack on methyl ethylene phosphate, a different but related monoanionic system. This was found to occur from the transition state that has an axial hydroxyl group to place it in an equatorial position.

In the case of methanol as a nucleophile, a transition state that corresponds clearly to the rotation of the proton around the P−O equatorial bond is identified. The attack of methanol on ethylene phosphate was previously studied by Lim and Tole at the HF/3-21+G* level, and a transition state for proton rotation was observed by them.[64]

The proton rotation leads to a different intermediate (Int_b, Figure 4) where the proton is now oriented toward the leaving group oxygen, thus facilitating its departure through the final (TS2) transition state. The intermediates after proton rotation Int_b are identified both in the case of OH^- and CH_3O^- as nucleophiles.

The final (TS2) transition states correspond to the breaking of the axial endocyclic P−O bond (see Figure 4). The bond breakage is accompanied by a proton transfer to the leaving group oxygen. The proton is closer to the equatorial oxygen and further from the leaving group axial oxygen in TS2 than in TS1 for exocyclic cleavage (see Tables 4 and 5). In fact, the distance between the O_{phos} and the hydrogen is only slightly elongated with respect to what is observed in the stable intermediate. Correspondingly, the distance between the hydrogen and the leaving apical oxygen is significantly longer (1.70−1.75 Å) than in the exocyclic TS (1.4−1.5 Å). The H−O−H angles deviate even more from linearity in the endocyclic TS (120−125°), and the O−O distance between proton donor and acceptor are slightly longer, 0.1 Å. On the other hand, in the presence of a ribose ring, both exo and endo transition states are very similar, but the exo transition states are located slightly later in the reaction coordinate, the P−OC distances at the transition state being slightly longer for exo transition states, and correspondingly, the proton transfer is slightly more advanced at exo transition states than at endo ones.

TABLE 6: Neutral Reaction. Relative Energies in the Gas-Phase with Respect to the Separate Reactants for the XOH + EPH/REPH Reactions (X = CH_3, H)

	reaction: HOH + EPH					reaction: CH_3OH + EPH				
	ΔE_e	ΔE_0	ΔH	ΔG	ΔG_{aq}	ΔE_e	ΔE_0	ΔH	ΔG	ΔG_{aq}
HB	−12.06	−9.40	−10.24	−0.55	10.81	−12.46	−10.60	−10.79	−0.62	12.20
$TS1_{dd}$	28.02	28.01	26.61	38.08	41.62	26.56	25.46	24.73	37.18	43.33
$TS1_{ud}$	25.64	26.45	24.72	36.92	42.60	25.33	24.96	23.99	37.12	43.71
Int_{du}	−0.20	3.43	1.98	13.54	17.86	2.97	5.61	4.74	17.73	23.93
Int_{dd}	0.76	4.61	3.04	14.98	19.03	2.94	5.68	4.76	17.89	23.95
Int_{ud}	−0.20	3.43	1.98	13.54	17.71	−0.57	2.32	1.35	14.61	22.27
Int_{uu}	1.65	5.30	3.83	15.51	17.72	1.69	4.37	3.50	16.50	23.24
$TSInt_u$	6.03	9.32	7.49	19.96	23.74	8.28	10.13	9.10	22.36	28.07
$TSInt_d$	5.77	8.98	7.20	19.52	24.16	7.10	9.27	8.09	21.87	28.97
$TS2_{du}$	19.75	20.26	18.67	30.68	36.56	22.18	21.41	20.59	33.45	39.63
$TS2_{uu}$	15.10	15.64	14.03	26.00	37.95	13.71	13.55	12.57	25.66	39.90
PROD	−9.48	−7.21	−7.82	1.35	9.80	−11.05	−9.42	−9.48	0.82	11.23
	reaction: HOH + REPH					reaction: CH_3OH + REPH				
	ΔE_e	ΔE_0	ΔH	ΔG	ΔG_{aq}	ΔE_e	ΔE_0	ΔH	ΔG	ΔG_{aq}
HB	−12.09	−9.46	−10.30	−0.66	8.87	−12.47	−10.62	−10.23	−2.43	8.25
$TS1_{du}^{Exo}$	25.98	26.86	25.66	36.64	39.43	25.71	25.37	24.95	36.81	40.09
$TS1_{dd}^{Exo}$	28.49	28.41	27.61	37.60	38.56	26.93	25.87	25.68	36.76	42.06
$TS1_{dd}^{Endo}$	28.24	28.14	27.34	37.23	38.06	26.66	25.54	25.38	36.40	40.84
$TS1_{ud}^{Endo}$	25.75	26.68	25.46	36.39	39.50	25.46	25.09	24.69	36.37	41.50
Int_{du}	0.10	3.77	2.86	13.19	15.10	2.99	5.68	5.34	17.16	20.42
Int_{dd}	1.07	4.88	3.89	14.30	15.97	3.12	5.89	5.53	17.31	19.83
Int_{ud}	0.21	3.89	3.00	13.03	15.55	−0.19	2.81	2.36	14.53	19.92
Int_{uu}	1.90	5.48	4.61	14.52	13.57	1.86	4.61	4.29	15.83	18.51
$TSInt_u^{Exo}$	5.43	8.71	7.44	18.43	18.34	7.13	9.16	8.63	20.66	23.83
$TSInt_d^{Exo}$	4.30	7.61	6.30	17.12	17.64	7.01	8.98	8.47	20.50	23.29
$TSInt_u^{Endo}$	5.74	9.03	7.76	18.89	19.13	8.55	10.59	10.06	22.20	24.73
$TSInt_d^{Endo}$	5.21	8.56	7.26	18.58	19.76	7.28	9.39	8.82	21.09	24.97
$TS2_{ud}^{Exo}$	20.49	21.00	19.99	30.56	34.44	19.53	19.15	18.79	30.41	36.38
$TS2_{uu}^{Exo}$	15.68	16.20	15.20	25.69	34.62	14.01	13.89	13.48	25.24	36.93
$TS2_{du}^{Endo}$	20.89	21.33	20.31	30.95	33.98	23.30	22.36	22.17	33.47	37.48
$TS2_{uu}^{Endo}$	16.17	16.53	15.54	26.02	34.95	14.61	14.23	13.91	25.28	36.12
PROD	−7.02	−4.27	−4.52	3.91	9.19	−8.68	−6.72	−6.32	3.30	11.22

As for TS1, two TS2 are identified (with exo and endo position of equatorial hydrogen, cf. Figure 4); they are similar in energy and they are lower in energy than the other TS by 10 kcal/mol, and thus not rate limiting (cf. Table 3 and Figure 4).

From this transition state, the rupture of the endocyclic P−O axial bond occurs, together with the transfer of the hydrogen on the leaving group oxygen. This yields a product with a charged phosphate group and neutral ribose ring, as expected. In the gas phase, an intramolecular H bond remains formed in this product between the ribose hydroxyl and a phosphoryl oxygen. This internal hydrogen bond stabilizes the reaction product in the gas phase, so that overall, and contrary to the dianionic case, the reaction is exothermic. More extended geometries in which the internal hydrogen bond is broken are higher in energy by around 10 kcal/mol (data not shown).

3.2.2. Solution Profile. As for the dianionic case, some important changes are observed when ΔG^i_{aq} and ΔG^i_{gas} are compared, which highlight the consideration of the solvent to understand these reactions. For the monoanionic species, the free energy of solvation of the gas-phase stationary points on the potential energy surface is generally less favorable than the solvation of the separate reactants (see Table 3), as expected, because the complexes have the same charge as the reactants and have larger radii.

The consequence is that the activation barrier for the monoanionic reactions increases by about 5−10 kcal/mol when passing from gas phase to solution. The magnitude of this solvation effect is smaller than what was observed for the dianionic species (see Tables 3 and S12). Therefore, the main effect of solvation is to bring the activation free energies for the monoanionic and dianionic reactions much closer than in the gas phase. Thus, for example for $CH_3O(H)$ attack on 2′,3′-ribose ethylene phosphate, we have a gas-phase free energy barrier of 92.98 and 34.18 kcal/mol for dianionic and monoanionic reactions, respectively. However, in solution, the barriers are 45.83 and 43.96 kcal/mol. Thus the barriers differ by about 60 kcal/mol in the gas phase, but only about 2 kcal/mol in solution. These results are in agreement with previous ab initio studies.[3,5,9,11,12,27,31]

Solvation data presented here are single-point energetic estimates on gas-phase structures, and explicit geometry optimization in solution could result in somewhat different structures. The region of the gas-phase potential energy surface, where structures are likely to be affected by solvation, are the stable H-bonded complex forming at the beginning of the gas-phase reaction, which is unlikely to form in solution, as there will be competition from water molecules forming H-bonds with both reactants. The transition state for proton rotation that connects the two intermediates is better solvated than the other transition states, which is expected in view of its smaller size and hydrogen atom pointing toward the solvent, and so the rotation profile could be affected by solvation. (cf. Figure 4 and Tables 3 and S12).

3.3. Neutral Reaction Mechanism. *3.3.1. Gas-Phase Profile.* The neutral reaction corresponds to the attack of water (or methanol) on the protonated phosphate. Although phosphates will be anionic at physiological (neutral) pH, acid-catalyzed hydrolysis can proceed through the neutral mechanism at very low pH (i.e., for instance, the pK_a of dimethyl phosphate is 1.29[27]). Moreover, phosphorane intermediates are more basic than phosphates[19,27] so that neutral phosphoranes can be relevant to reactions at near-neutral pH. Relative energies with respect

TABLE 7: P−O Axial Bond Distances (Å) and Angle (deg) for All the Stationary Points Characterized for the XOH + (R)EPH Reactions Using B3LYP/6-31+G(d,p) Level of Theory

	HOH + EPH			CH_3OH + EPH		
	P−OX	P−OC	O_{ax}−P−O_{ax}	P−OX	P−OC	O_{ax}−P−O_{ax}
HB	3.247	1.626	135.2	3.240	1.627	127.6
$TS1_{dd}$	2.137	1.637	173.2	2.091	1.641	172.6
$TS1_{ud}$	1.956	1.678	179.2	1.936	1.685	178.4
Int_{du}	1.677	1.724	197.6	1.673	1.729	175.2
Int_{dd}	1.726	1.680	176.8	1.723	1.686	179.7
Int_{ud}	1.677	1.724	179.6	1.674	1.727	179.6
Int_{uu}	1.644	1.790	177.7	1.638	1.798	178.2
$TSInt_u$	1.641	1.734	157.8	1.656	1.754	172.7
$TSInt_d$	1.687	1.675	157.8	1.677	1.688	156.0
$TS2_{du}$	1.641	2.070	175.6	1.626	2.130	172.5
$TS2_{uu}$	1.600	2.289	173.9	1.589	2.320	173.9
PROD	1.612	3.414	150.8	1.602	3.478	146.8
	HOH + REPH			CH_3OH + REPH		
	P−OX	P−OC	O_{ax}−P−O_{ax}	P−OX	P−OC	O_{ax}−P−O_{ax}
HB	3.253	1.624	132.2	.244	1.625	132.2
$TS1_{du}^{Exo}$	1.950	1.678	178.8	1.930	1.685	178.6
$TS1_{dd}^{Exo}$	2.141	1.636	173.5	2.099	1.642	173.2
$TS1_{dd}^{Endo}$	2.132	1.635	172.8	2.091	1.641	172.6
$TS1_{ud}^{Endo}$	1.952	1.679	179.4	1.931	1.686	178.5
Int_{du}	1.675	1.724	1.781	1.670	1.731	174.5
Int_{dd}	1.724	1.681	177.0	1.721	1.687	179.2
Int_{ud}	1.676	1.727	178.9	1.672	1.732	179.6
Int_{uu}	1.642	1.791	176.3	1.636	1.802	177.1
$TSInt_u^{Exo}$	1.642	1.736	158.6	1.642	1.747	160.1
$TSInt_d^{Exo}$	1.668	1.694	157.5	1.689	1.691	161.7
$TSInt_u^{Endo}$	1.643	1.738	159.8	1.653	1.759	170.7
$TSInt_d^{Endo}$	1.683	1.673	156.2	1.688	1.689	160.6
$TS2_{ud}^{Exo}$	1.639	2.067	176.8	1.629	2.093	178.2
$TS2_{uu}^{Exo}$	1.597	2.323	174.1	1.590	2.335	176.1
$TS2_{du}^{Endo}$	1.638	2.081	176.2	1.623	2.157	172.4
$TS2_{uu}^{Endo}$	1.597	2.323	174.1	1.586	2.359	174.1
PROD	1.602	3.320	124.4	1.591	3.326	124.6

to the separate neutral reactants (protonated phosphate and water/methanol) can be found in Table 6, and relevant geometrical information is found in Tables 7 and 8. Full information on solvation free energies and aqueous free energy barriers with various theoretical levels can be found in the Supporting Information.

The reaction profile for the neutral reaction resembles in many aspects that of the monoanionic reaction mechanism. However, as both the nucleophile and phosphate are protonated, the number of isomers for the transition states are twice that observed for the monoanionic reactions because the two protons that become bound to the equatorial oxygens can assume two different orientations (see Figure 5 and discussion below). The first step of the neutral reaction in the gas phase is the formation of a stable hydrogen-bonded (HB) complex. However, these kind of complexes are kinetically irrelevant, especially in aqueous solution where positive free aqueous energies are calculated with respect to the infinitely separated reactants. The reaction then proceeds to the TS for exocyclic cleavage. Four distinct TS are identified when a ribose ring is present. All of them correspond to a nucleophilic attack on the phosphorus atom coupled with a proton transfer from the nucleophile to one of the equatorial oxygens. This type of mechanism in which P−O bond formation/rupture is coupled with proton transfer between phosphoryl oxygen and nucleophile has also been considered based on the β_{lg} values of leaving groups on the cleavage of RNA neutral phosphodiesters,[58] which are only slightly negative and thus suggest that the leaving group in these reaction departs as an alcohol. In the case of a ribose ring present, we classified the two equatorial oxygens as being exo or endo with respect to the ribose ring, and therefore, there are two exo and two endo transition states (see Figure 5), classified according to the equatorial oxygen that receives the proton in the transition state. For each of the exo and endo transition states, there are two possibilities, depending on the orientation of the other equatorial proton (the one that is already present in the phosphate reactant). As a result, in two of the TS1 transition states, $TS1_{dd}^{exo}$ and $TS1_{dd}^{endo}$, both protons attached to the equatorial oxygens points toward the nucleophile, while in the two other transition states, $TS1_{du}^{exo}$ and $TS1_{ud}^{endo}$, one proton points toward the nucleophile and the other toward the leaving group. The energies of the different transition states with respect to the reactants (see Table 6) do not differ much, even when comparing the reaction with different nucleophiles and with/without ribose ring. All the gas-phase free energy barriers lie within 36−38 kcal/mol. Larger differences are observed in the geometries (see Tables 7 and 8). When both equatorial protons are pointing toward the nucleophile, the P−O axial distance to the nucleophile O is longer, around 2.1 Å, than when one proton points up and the other down, around 1.95 Å (cf. Table 7). These P−O axial distances are shorter than in the monoanionic (longer than 2.2

TABLE 8: Proton Transfer between Oxygens at the Transition States[a]

	HOH + EPH				CH_3OH + EPH			
	H−O_X	H−O_P	H−O-CH_2^-	O−H−O	H−O_X	H−O_P	H−O-CH_2^-	O−H−O
$TS1_{dd}$	1.308	1.147		133.3	1.255	1.185		131.7
$TS1_{ud}$	1.199	1.269		129.2	1.196	1.265		127.6
$TS2_{du}$		1.202	1.247	133.1		1.177	1.273	135.2
$TS2_{uu}$		1.112	1.376	138.7		1.093	1.413	138.8
	HOH + REPH				CH_3OH + REPH			
	H−O_X	H−O_P	H−O-CH_2^-	O−H−O	H−O_X	H−O_P	H−O-CH_2^-	O−H−O
$TS1_{du}^{Exo}$	1.199	1.272		129.0	1.197	1.266		127.5
$TS1_{dd}^{Exo}$	1.201	1.148		132.5	1.259	1.182		131.8
$TS1_{dd}^{Endo}$	1.298	1.152		132.7	1.255	1.185		131.7
$TS1_{ud}^{Endo}$	1.199	1.271		129.0	1.196	1.265		127.5
$TS2_{ud}^{Exo}$		1.205	1.243	133.9		1.205	1.243	133.9
$TS2_{uu}^{Exo}$		1.118	1.367	140.1		1.094	1.413	138.6
$TS2_{du}^{Endo}$		1.218	1.232	133.2		1.183	1.265	135.9
$TS2_{uu}^{Endo}$		1.118	1.367	140.1		1.099	1.402	140.4

[a] H−O_X is the distance in Å between the proton and the oxygen of the nucleophile (water or methanol), H−O_P refers to the distance between the proton and the corresponding equatorial phosphoryl oxygen, H−O−CH_2^- is the distance between the transfered proton and the axial O−CH_2^- group. O−H−O angle is the angle of the proton transfer, in degrees.

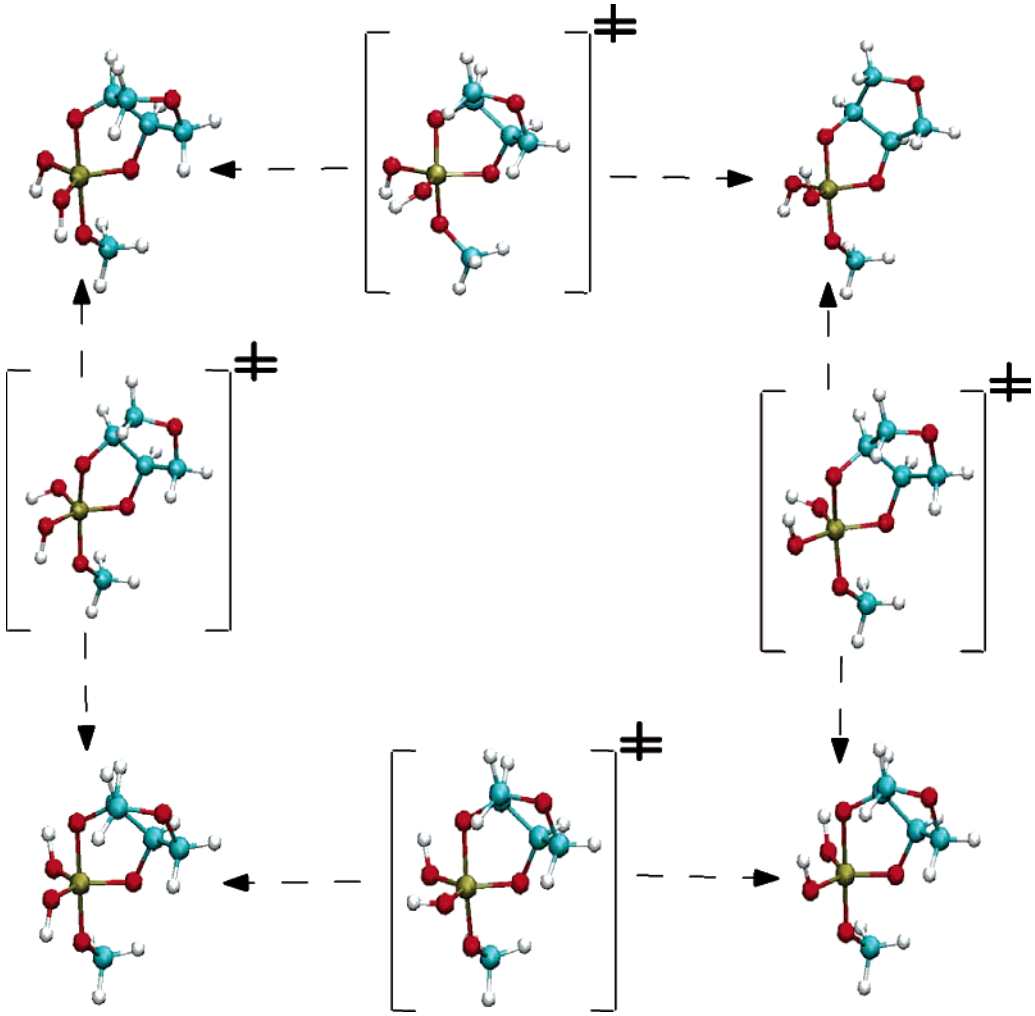

Figure 6. Transition states connecting the intermediates in the neutral potential energy surface.

Å, see Table 4) or dianionic case (around 2.6 Å, Table 2). An important conclusion, therefore, is that the degree of associative/dissociative character is highly influenced by the protonation state of the system, augmenting the associative character of the transition states as the total charge decreases. The geometry for proton transfer in the TS also differs between the monoanionic and neutral cases. In the neutral TS1s, the proton from the incoming nucleophile is almost equidistant from the nucleophile oxygen and the phosphoryl oxygen (see Table 8), while in the monoanionic case (Table 5), the distance to the equatorial O is much shorter than that to the nucleophile O. It is remarkable to note that β_{lg} values for the transesterification cleavage of neutral phosphodiesters[58] are less negative, namely -0.12, than for monoanionic phosphodiesters, -0.59, consistent with a higher degree of proton sharing between the nucleophile and the phosphoryl oxygen at the neutral transition states than in monoanionic reactions. The reaction then proceeds to the formation of stable neutral phosphorane intermediates. There are four distinct neutral phosphorane intermediates, depending on the orientation of the protons at the phosphoryl equatorial oxygens (see Figure 5), labeled as INT_{du}, INT_{dd}, INT_{du}, and INT_{uu}. We notice, however, that barriers for the connection of these intermediates are small and much lower in every case than the barriers implied by TS1 or TS2 (exo and endocyclic cleavage) type transition states. All the phosphorane intermediates lie very close in energy. In general, the following trend is observed: (i) alternate orientation of the protons, ud or du, is favored (ii) intermediates resultant from water attack show somewhat lower relative energies than intermediates resultant from methanol attack, especially for the intermediates that show the equatorial protons oriented toward the nucleophile ("down" orientation), in agreement with the results obtained in ref 27. All these intermediates can be formally connected by transition states corresponding to different single equatorial proton rotations, as shown schematically in Figure 6. However, we found that, in many cases, these rotations were coupled with pseudorotation of the whole structure at the transition state (TSINT transition states). Transition states with a significant pseudorotation character show $O_{ax}-P-O_{ax}$ angles around 160°. A full discussion of these types of transition states are beyond the scope of the present paper, but an interesting discussion of pseudorotation processes in oxyphosphoranes can be found in ref 25. Barriers for the connection of these intermediates are small and much lower in every case than the barriers implied by in-line TS1 or TS2 (exo and endocyclic cleavage) type transition states. From the neutral intermediates, the reaction can proceed to endocyclic cleavage, only if at least one proton is oriented toward the leaving group so as to protonate it. Four transition states that have the proton in this orientation are identified (cf. Figure 6). Again, when a ribose ring is presented, the transition states can be classified exo or endo, depending on whether the proton transfer to the leaving group is exo or endo. Overall, these TS for endocyclic cleavage are lower in energy than those for exocyclic cleavage (by about 6 kcal/mol), and thus, they are not rate limiting. In the neutral TS2's, the proton is shared between the leaving group oxygen and one equatorial oxygen,

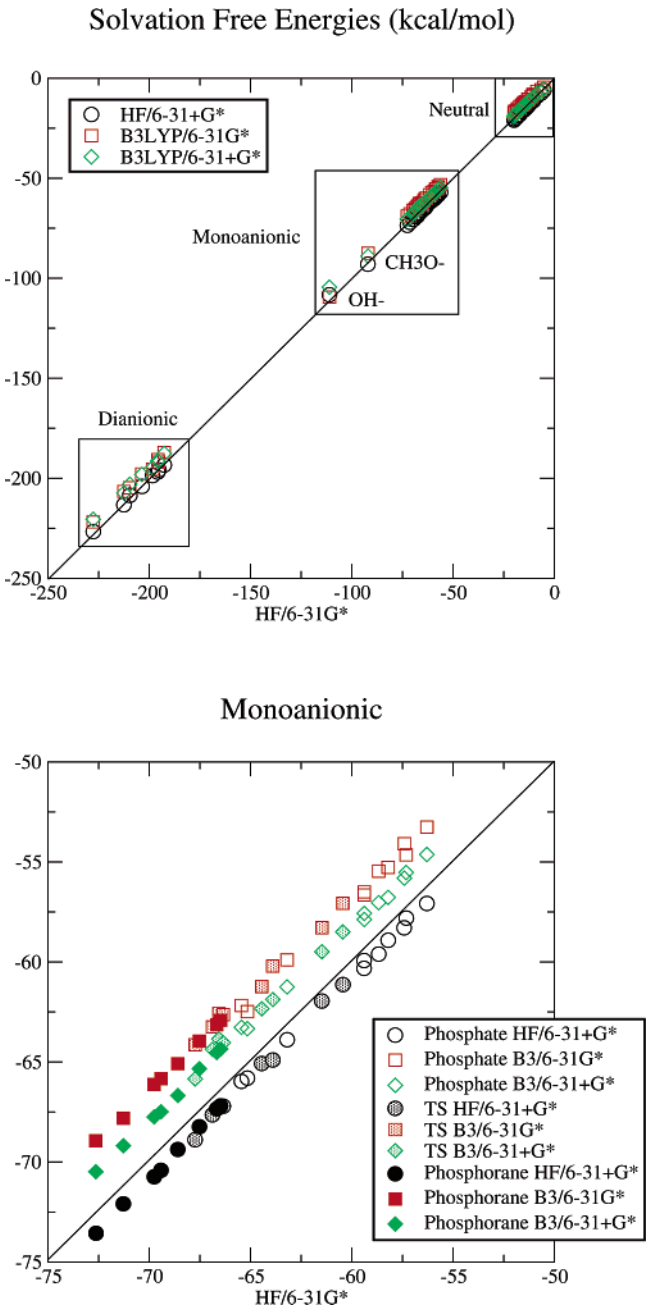

Figure 7. Top diagram: comparison of the HF/6-31G* solvation free energies (in kcal/mol) for the different compounds with solvation free energies at HF/6-31+G*, B3LYP/6-31G*, and B3LYP/6-31+G*. Top diagram shows how qualitative trends are conserved among the different methods. Notice how the solvation free energies can be clustered according to the total charge of the compound. Bottom diagram: solvation free energies for the monoanionic phosphates and phosphoranes species shown in detail.

as was already observed for the TS1's (cf. Table 8 and Figure 5). The products are finally formed by cleavage of the P−OC bond and simultaneous transfer of one of the phosphoryl hydrogens to the leaving group. An internal H bond is maintained, as for the monoanionic case. The reactions energetics of the neutral and monoanionic reactions are similar in the gas phase (see Tables 3 and 6).

3.3.2. Solution Profile. Solvation has a relatively minor effect on the reaction energetics of the neutral reaction (see Table 6), as compared to monoanionic or dianionic reactions. Solvation, nevertheless, tends to favor the separated reactants, and therefore, we obtain higher relative energies in solution than in the gas phase. The hydrogen-bonded complexes formed at the beginning and end of the gas-phase reaction are significantly destabilized by solvation, suggesting that they would not occur in solution; a geometry optimization would be needed to confirm that they remain present in water. As for the transition states and intermediates, they also show higher relative energies in solution, but the favorable solvation free energy of separated reactants is somewhat balanced by the higher polarization of the P−O bonds in phosphorane structures than in tetravalent phosphate species. Overall, the shape of the neutral reactions are very similar to that of the monoanionic reactions. However, the energies and free energies of the neutral phosphorane intermediates with respect to the neutral reactants differ from the monoanionic case (see Table 6), the neutral phosphoranes being significantly more stable, between 14 and 24 kcal/mol for neutrals and between 25 and 30 kcal/mol for monoanionic ones. Therefore, an important consequence is that the barrier for the dissociation of the intermediates into products/reactants is significantly higher for the neutral than for the monoanionic reaction path. This, along with the low barriers for the interconversion among intermediates, suggests that neutral phosphorane intermediates will show sufficient lifetime to pseudorotate, and therefore, the endocyclic cleavage reaction can be proceed from various possible intermediates.

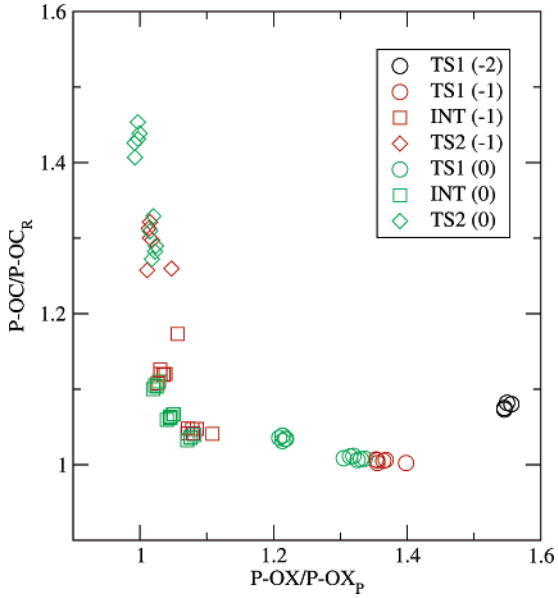

Figure 8. Axial P−O interatomic distances with respect to reference values in the product (P) and reactant (R) at each TS1, INT, and TS2 structures.

3.4. Reaction Pathways of Cyclic Phosphodiesters. The hydrolysis of phosphodiesters is generally thought to follow an associative mechanism (see refs 65−67 and refs cited therein), and the stationary points identified here for the hydrolysis reactions of cyclic phosphodiesters clearly agree with that view. Significant differences in the structures of the transition states according to the total charge are nevertheless observed, and it is of interest to examine the degree of bond breaking/forming at the different stationary points along the reaction pathway. We compared the bond lengths between the nucleophile/leaving group and phosphorus in the transition states and intermediates with their values in the product or reactants, respectively (see Figure 8). Significant bond formation occurs between the nucleophile and phosphorus in the rate-limiting transition states for hydrolysis, while the distance to the leaving group is only slightly increased with respect to the distance in the reactants. This is the hallmark of an associative mechanism,[68] confirming

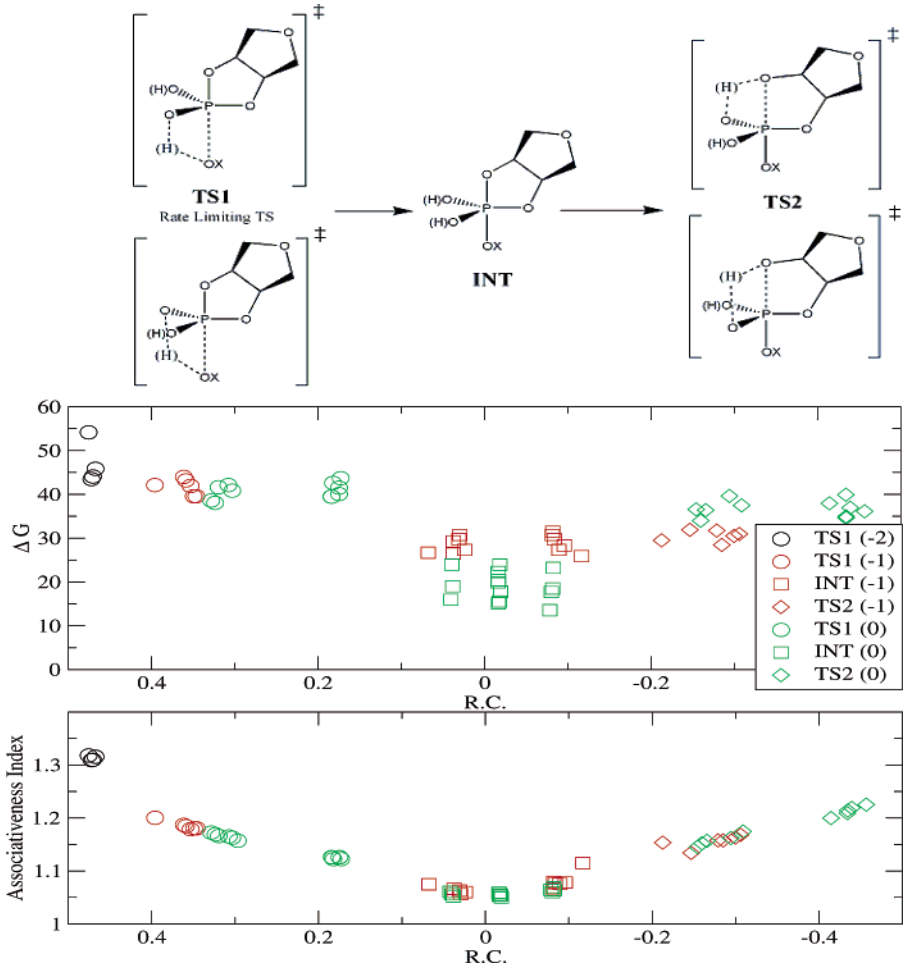

Figure 9. Relative aqueous free energies with respect to separate reactants as a function of a reaction coordinate (RC) defined as P−OX/P−OX$_P$ − P−OC/P−OC$_R$. P−OC and P−OX are the two axial P−O interatomic distances, P−OC is the P−O distance with the leaving group and P−OX with the nucleophile. The two reference values P−OC$_R$ and P−OX$_P$ are the corresponding phosphate bonds in the reactant (R) and product (P), respectively. This reaction coordinate can be interpret as the difference between the degree of phosphorus−nucleophile bond formation and bond cleavage with the leaving group for a given structure. Bottom diagram represents the degree of associativeness of the structure as defined as $^1/_2$*(P−OX/P−OXP + P−OC/P−OC$_R$). A value of one represents the maximum degree of associativeness, and values larger than one indicate a higher dissociative character of the structure.

early experimental studies in which it was remarked that dissociative mechanism is highly unlikely for the hydrolysis of phosphodiesters.[65] More recent ^{18}O kinetic isotope studies[55] and determination of β_{lg} Bronsted-type slopes for the cleavage of hydroxide-ion-catalyzed RNA phosphodiester bonds[57−59,69] also support an associative mechanism even for the dianionic reaction. However, the degree of bond forming to the nucleophile varies significantly with the total charge, with the dianionic reaction having the longest P−OX distance and, hence, the least associative transition state. For the monoanionic and neutral reactions, the transition state occurs with more bond formation to the nucleophile than in the dianionic reaction. It can, however, be seen that the elongation of the bond lengths in the transition states with respect to the reactant/product value (cf. Figure 9a) remains small in all cases (it is at most 30% for the dianionic case), which is in agreement with the associative character of the reactions. Interestingly, for the neutral reactions, the orientation of the equatorial protons (cf. Figures 4 and 5) influences the geometry of the transition states: when both protons are oriented toward the nucleophile, the transition state occurs earlier (i.e., with less bond formation between the nucleophile and phosphorus) than when one of the protons is oriented toward the leaving group. This is in accord with the Hammond postulate.[16,70] For the neutral and monoanionic reactions, the reaction proceeds through the formation of phosphorane intermediates, and in those cases, the bonds to both the nucleophile and leaving group are only at most 10% longer than in the reactants/products. The formation of these stable phosphoranes is also a clear indication of an associative mechanism. For the neutral and monoanionic reactions, departure of the leaving group occurs from the intermediates, while the bond to the nucleophile remains close to the product value. The elongation in the transition states for leaving group departures (TS2, cf. Figures 4 and 5) is at most 25% of the reactant/product state. The link between the geometries and energies is presented in Figure 9. The calculated activation barriers with respect to the separate reactions are similar for all reactions. The intermediates clearly appear as low-energy structures and increased stability of the neutral phosphoranes is seen. For the neutral and monoanionic reactions, the rate-determining transition state is always that for attack of the nucleophile rather than departure of the leaving group. For the dianionic mechanism, the transition state also corresponds to attack of the nucleophile rather than departure of the leaving group. This seems to be coherent with experimental kinetic analysis[59,69] of isomerization and cleavage reactions of RNA phosphodiesters. Quantitative estimates of reaction barriers would require more detailed calculations, including geometry optimization in solution (see ref 18) and the possibility of water-mediated proton transfer, which has been shown to play an

important role in facilitating the proton transfer in monoanionic and neutral reactions.[55]

4. Concluding Discussion

We present an extensive computational study of a variety of cyclic phosphodiester hydrolysis reactions. The calculations and discussion focus on the most relevant stationary points of each potential energy surface to explain the in-line mechanism for this set of biologically important reactions. From our systematic studies, we confirm that the transition state corresponding to the initial attack of the nucleophile on the phosphate is the rate-limiting transition state of the reaction. This trend is preserved regardless of the particular nucleophile, the presence/absence of a ribose ring in the model phosphate, or the inclusion of solvent effects. The total charge of the system is the main factor that determines the energetic trends in the gas phase: the largest barriers are for the dianionic mechanism, while the monoanionic and neutral reactions have similar energetics and smaller barriers. Another important effect of the total charge is the existence and stability of phosphorane intermediates. No gas-phase intermediates are observed for the dianionic reaction. Monoanionic intermediates are found in the gas phase, but the barrier for their dissociation to the products is very low. Neutral phosphorane intermediates, on the other hand, have larger barriers for dissociation to both reactants and products, which suggests that they could have a significant lifetime in the gas phase. Phosphoranes that have kinetically significant lifetimes can undergo protonation/deprotonation from solvent or pseudorotation that could alter the stereochemical outcome of the reaction and lead to products involving migration.[1,2,31] The data presented here are thus coherent with the observation that isomerization reactions leading to migration products are catalyzed under acidic conditions[1] (which favor neutral phosphoranes). The total charge also influences the geometry of the transition states and intermediates.

All the reactions presented here correspond to an associative mechanism, yet differences are observed as a function of the total charge. The rate-limiting transition state becomes gradually more associative, with P−OX bonds decreasing by 0.69 Å and $P-O_{ax}$ by 0.17 Å when going from the −2 to the neutral reaction. Concurrently, the angles approach linearity as the negative charge of the system decreases. Thus, the average for monoanionic intermediates is 161.9°, whereas for neutral intermediates, it is 178.4°. Solvent has a dramatic effect on the relative energies with respect to the infinitely separated reactants and serves to equalize the barriers for the dianionic, monoanionic, and neutral mechanisms. Our calculations also highlight similarities with the hydrolysis mechanism of noncyclic phosphate such as monomethyl[15,36] and dimethyl phosphate.[71] Indeed, in an early study of the mechanism for associative monomethyl phosphate hydrolysis in gas phase and in solution,[15,36] it was observed that the monoanionic and neutral reaction mechanisms proceed by proton transfer from the nucleophile to the phosphate reactant, and that solvation raises the activation barrier for the neutral and monoanionic reactions, while it leads to a significant lowering of activation free energy for the dianionic case. A recent study[71] of the dianionic and monoanionic mechanism for the hydrolysis of dimethyl phosphate reached similar conclusions. Our work also shows that, for the monoanionic and neutral reactions, proton transfer from the nucleophile to the phosphate is an essential step of the reaction. Moreover, we characterized various isomers of the monoanionic and neutral transition states and showed that, for ribose ethylene phosphate, both exo and endo proton transfer lead to very similar barriers.

Isomerization of the protonated phosphoranes plays an essential role in the reaction pathway and is associated with significant energy barriers in the gas phase. This is a point that is important for enzyme-catalyzed reactions; i.e., it shows that, for neutral and monoanionic reactions, the orientation of protons attached to the equatorial oxygen has an important role in facilitating attack/departure of the nucleophiles and that the change in proton orientation is a component of the reaction path that should not be overlooked.

This work has implications for mechanistic interpretation of phosphate hydrolysis in biological systems, particularly in RNA hydrolysis where cyclic phosphate intermediates are commonly encountered. In enzymatic systems, it is often postulated that a general acid protonates the phosphate and/or a base activates the nucleophile. Here, it is seen that, in the simple gas-phase model system constituted of phosphate and nucleophile, the nucleophile acts as the general acid and the phosphate as the general base. These data provide important insights into the intrinsic reactivity of the phosphates in the absence of surrounding enzyme or solvent and, therefore, provide a reference point for understanding more complex systems in which catalysis occurs. It can also be taken as a high-level density functional theory dataset of reactions for which more approximate models, such as focused semiempirical treatments, can be developed and tested.

Acknowledgment. X.L. is grateful for the financial support provided by Euskal Herriko Unibertsitatea (the University of the Basque Country), Gipuzkoako Foru Aldundia (the Provincial Government of Guipuzkoa), Eusko Jaurlaritza (the Basque Government), and the Spanish Office for Scientific Research. The SGI/IZO-SGIker UPV/EHU (supported by the National Program for the Promotion of Human Resources within the National Plan of Scientific Research, Development, and Innovation−Fondo Social Europeo and MCyT) is gratefully acknowledged for generous allocation of computational resources. D.Y. is grateful for financial support provided by the National Institutes of Health (Grant 1R01-GM62248-01A1). A.D. is grateful for financial support provided by the Centre National de la Recherche Scientifique (CNRS), the Institut National de la Santé et de la Recherche Médicale (INSERM), and the Université L. Pasteur de Strasbourg. Computational resources were provided in part by the Minnesota Supercomputing Institute and in part by the Centre Informatique National de l'Enseignement Supérieur (CINES) and the Institut du Développement et des Ressources en Informatique Scientifique (IDRIS). The part of the work done at Harvard University was supported by the National Institutes of Health.

Supporting Information Available: Full information on solvation free energies and aqueous free energy barriers with various theoretical levels. This material is available free of charge via the Internet at http://pubs.acs.org.

References and Notes

(1) Oivanen, M.; Kuusela, S.; Lönnberg, H. *Chem. Rev.* **1998**, *98*, 961−990.

(2) Perreault, D. M.; Anslyn, E. V. *Angew. Chem., Int. Ed. Engl.* **1997**, *36*, 432−450.

(3) Uchimaru, T.; Tanabe, K.; Nishikawa, S.; Taira, K. *J. Am. Chem. Soc.* **1991**, *113*, 4351−4353.

(4) Lim, C.; Karplus, M. *J. Am. Chem. Soc.* **1990**, *112*, 5872−5873.

(5) Lim, C.; Tole, P. *J. Phys. Chem.* **1992**, *96*, 5217−5219.

(6) Tole, P.; Lim, C. *J. Phys. Chem.* **1993**, *97*, 6212−6219.

(7) Tole, P.; Lim, C. *J. Am. Chem. Soc.* **1994**, *116*, 3922−3931.

(8) Chang, N.; Lim, C. *J. Phys. Chem. A* **1997**, *101*, 8706−8713.

(9) Dejaegere, A.; Lim, C.; Karplus, M. *J. Am. Chem. Soc.* **1991**, *113*, 4353−4355.
(10) Dejaegere, A.; Karplus, M. *J. Am. Chem. Soc.* **1993**, *115*, 5316−5317.
(11) Dejaegere, A.; Liang, X. L.; Karplus, M. *J. Chem. Soc., Faraday Trans.* **1994**, *90*, 1763−1770.
(12) Wladkowski, B. D.; Krauss, M.; Stevens, W. J. *J. Phys. Chem.* **1995**, *99*, 6273−6276.
(13) Wladkowski, B. D.; Krauss, M.; Stevens, W. J. *J. Am. Chem. Soc.* **1995**, *117*, 10537−10545.
(14) Glennon, T. M.; Warshel, A. *J. Am. Chem. Soc.* **1998**, *120*, 10234−10247.
(15) Florián, J.; Warshel, A. *J. Phys. Chem. B* **1998**, *102*, 719−734.
(16) Lopez, X.; Dejaegere, A.; Karplus, M. *J. Am. Chem. Soc.* **2001**, *123*, 11755−11763.
(17) Mercero, J. M.; Barrett, P.; Lam, C. W.; Fowler, J. E.; Ugalde, J. M.; Pedersen, L. G. *J. Comput. Chem.* **2000**, *21*, 43−51.
(18) Chen, X.; Zhan, C.-G. *J. Phys. Chem. A* **2004**, *108*, 6407−6413.
(19) Range, K.; McGrath, M. J.; Lopez, X.; York, D. M. *J. Am. Chem. Soc.* **2004**, *126*, 1654−1665.
(20) Gregersen, B. A.; Lopez, X.; York, D. M. *J. Am. Chem. Soc.* **2004**, *126*, 7504−7513.
(21) Gregersen, B. A.; Khandogin, J.; Thiel, W.; York, D. M. *J. Phys. Chem. B* **2005**, *109*, 9810−9817.
(22) López, C. S.; Faza, O. N.; Gregersen, B. A.; Lopez, X.; de Lera, A. R.; York, D. M. *ChemPhysChem* **2004**, *5*, 1045−1049.
(23) Liu, Y.; Lopez, X.; York, D. M. *Chem. Commun.* **2005**, *31*, 3909−3911.
(24) Liu, Y.; Gregersen, B. A.; Lopez, X.; York, D. M. *J. Phys. Chem. B* **2005**, *109*, 19987−20003.
(25) López, C. S.; Faza, O. N.; R. de Lera, A.; York, D. M. *Chem.—Eur. J.* **2005**, *11*, 2081−2093.
(26) Xu, D.; Guo, H.; Liu, Y.; York, D. M. *J. Phys. Chem. B* **2005**, *109*, 13827−13834.
(27) Lopez, X.; Schaefer, M.; Dejaegere, A.; Karplus, M. *J. Am. Chem. Soc.* **2002**, *124*, 5010−5018.
(28) Davies, J.; Doltsinis, N.; Kirby, A.; Roussev, C.; Sprik, M. *J. Am. Chem. Soc.* **2002**, *124*, 6594−6599.
(29) Lopez, X.; York, D. M.; Dejaegere, A.; Karplus, M. *Int. J. Quantum Chem.* **2002**, *86*, 10−26.
(30) Zhou, D.-M.; Usman, N.; Wincott, F. E.; Matulic-Adamic, J.; Orita, M.; Zhang, L.-H.; Komiyama, M.; Kumar, P. K. R.; Taira, K. *J. Am. Chem. Soc.* **1996**, *118*, 5862−5866.
(31) Zhou, D.-M.; Taira, K. *Chem. Rev.* **1998**, *98*, 991−1026.
(32) Tomasi, J.; Persico, M. *Chem. Rev.* **1994**, *94*, 2027−2094.
(33) Cossi, M.; Barone, V.; Cammi, R.; Tomasi, J. *Chem. Phys. Lett.* **1996**, *255*, 327−335.
(34) Mineva, T.; Russo, N.; Sicilia, E. *J. Comput. Chem.* **1998**, *19*, 290−299.
(35) Arantes, G. M.; Chaimovich, B. *J. Phys. Chem. A* **2005**, *109*, 5625−5635.
(36) Florián, J.; Warshel, A. *J. Am. Chem. Soc.* **1997**, *119*, 5473−5474.
(37) Hu, C.-H.; Brinck, T. *J. Phys. Chem. A* **1999**, *103*, 5379−5386.
(38) Range, K.; Riccardi, D.; Cui, Q.; Elstner, M.; York, D. M. *Phys. Chem. Chem. Phys.* **2005**, *7*, 3070−3079.
(39) López, C. S.; Faza, O. N.; Coss×c6o, F. P.; York, D. M.; de Lera, A. R. *Chem.—Eur. J.* **2005**, *11*, 1734−1738.
(40) Liu, Y.; Gregersen, B. A.; Hengge, A.; York, D. M. *Biochemistry*, submitted for publication.
(41) Range, K.; López, C. S.; Moser, A.; York, D. M. *J. Phys. Chem. A* **2006**, *110*, 791−797.
(42) Becke, A. D. *J. Chem. Phys.* **1993**, *98*, 5648−5652.
(43) Lee, C.; Yang, W.; Parr, R. G. *Phys. Rev. B.* **1988**, *37*, 785−789.
(44) Curtiss, L. A.; Jones, C.; Trucks, G. W.; Raghavachari, K.; Pople, J. A. *J. Chem. Phys.* **1990**, *93*, 2537−2545.
(45) Curtiss, L. A.; Carpenter, J. E.; Raghavachari, K.; Pople, J. A. *J. Chem. Phys.* **1992**, *96*, 9030−9034.
(46) Frisch, M. J.; Trucks, G. W.; Schlegel, H. B.; Scuseria, G. E.; Robb, M. A.; Cheeseman, J. R.; Zakrzewski, V. G.; Montgomery, J. A., Jr.; Stratmann, R. E.; Burant, J. C.; Dapprich, S.; Millam, J. M.; Daniels, A. D.; Kudin, K. N.; Strain, M. C.; Farkas, O.; Tomasi, J.; Barone, V.; Cossi, M.; Cammi, R.; Mennucci, B.; Pomelli, C.; Adamo, C.; Clifford, S.; Ochterski, J.; Petersson, G. A.; Ayala, P. Y.; Cui, Q.; Morokuma, K.; Malick, D. K.; Rabuck, A. D.; Raghavachari, K.; Foresman, J. B.; Cioslowski, J.; Ortiz, J. V.; Stefanov, B. B.; Liu, G.; Liashenko, A.; Piskorz, P.; Komaromi, I.; Gomperts, R.; Martin, R. L.; Fox, D. J.; Keith, T.; Al-Laham, M. A.; Peng, C. Y.; Nanayakkara, A.; Gonzalez, C.; Challacombe, M.; Gill, P. M. W.; Johnson, B. G.; Chen, W.; Wong, M. W.; Andres, J. L.; Head-Gordon, M.; Replogle, E. S.; Pople, J. A. *Gaussian 98*; Gaussian, Inc.: Pittsburgh, PA, 1998.
(47) Hehre, W.; Radom, L.; von Schleyer, P.; Pople, J. *Ab Initio Molecular Orbital Theory*; John Wiley & Sons: New York, 1986.
(48) Cramer, C. J. *Essentials of Computational Chemistry: Theories and Models*, 2nd ed.; John Wiley & Sons: Chichester, England, 2002.
(49) Herbert, J. M.; Ortiz, J. V. *J. Phys. Chem. A* **2000**, *104*, 11786−11795.
(50) Tidor, B.; Karplus, M. *J. Mol. Biol.* **1994**, *238*, 405−414.
(51) Menegon, G.; Loos, M.; Chaimovich, H. *J. Phys. Chem. A* **2002**, *106*, 9078−9084.
(52) Iché-Tarrat, N.; Barthelat, J.-C.; Rinaldi, D.; Vigroux, A. *J. Phys. Chem. B* **2005**, *109*, 22570−22580.
(53) Barone, V.; Cossi, M.; Tomasi, J. *J. Chem. Phys.* **1997**, *107*, 3210−3221.
(54) Cramer, C. J.; Truhlar, D. G. *Chem. Rev.* **1999**, *99*, 2161−2200.
(55) Gerratana, B.; Sowa, G. A.; Cleland, W. W. *J. Am. Chem. Soc.* **2000**, *122*, 12615−12621.
(56) Gregersen, B. A.; Lopez, X.; York, D. M. *J. Am. Chem. Soc.* **2003**, *125*, 7178−7179.
(57) Kosonen, M.; Youseti-Salakdeh, E.; Strömberg, R.; Lönnberg, H. *J. Chem. Soc., Perkin Trans. 2* **1997**, 2611−2666.
(58) Mikkola, S.; Kosonen, M.; Lönnberg, H. *Curr. Org. Chem.* **2002**, *6*, 523−538.
(59) Lönnberg, H.; Strömberg, R.; Williams, A. *Org. Biomol. Chem.* **2004**, *2*, 2165−2167.
(60) Breslow, R. *Proc. Natl. Acad. Sci. U.S.A.* **1993**, *90*, 1208−1211.
(61) Kosonen, M.; Yousefi-Salakdeh, E.; Strömberg, R.; Lönnberg, H. *J. Chem. Soc., Perkin Trans. 2* **1998**, 1589−1595.
(62) Kosonen, M.; Seppänen, R.; Wichmann, O.; Lönnberg, H. *J. Chem. Soc., Perkin Trans. 2* **1999**, 2433−2439.
(63) Uchimaru, T.; Uebayasi, M.; Hirose, T.; Tsuzuki, S.; Yliniemelä, A.; Tanabe, K.; Taira, K. *J. Org. Chem.* **1996**, *61*, 1599−1608.
(64) Lim, C.; Tole, P. *J. Am. Chem. Soc.* **1992**, *114*, 7245−7252.
(65) Kirby, A. J.; Younas, M. *J. Chem. Soc. B* **1970**, 510−513.
(66) Åqvist, J.; Kolmodin, K.; Florian, J.; Warshel, A. *Chem. Biol.* **1999**, *6*, R71−R80.
(67) Knowles, J. *Science* **2003**, *299*, 2002−2003.
(68) Maegley, K.; Admiraal, S. J.; Herschlag, D. *Proc. Natl. Acad. Sci. U.S.A.* **1996**, *93*, 8160−8166.
(69) Lönnberg, T.; Lönnberg, H. *Curr. Opin. Chem. Biol.* **2005**, *9*, 665−673.
(70) Hammond, G. S. *J. Am. Chem. Soc.* **1955**, *77*, 334−338.
(71) Imhof, P.; Fischer, S.; Krämer, R.; Smith, J. C. *J. Mol. Struct. (THEOCHEM)* **2005**, *713*, 1−5.